processes

Article

Investigation of the Influence of Formation Water on the Efficiency of CO_2 Miscible Flooding at the Core Scale

Yanfu Pi [1], Zailai Su [1,*], Li Liu [1], Yutong Wang [2], Shuai Zhang [3], Zhihao Li [1] and Yufeng Zhou [1]

[1] Key Laboratory of Enhanced Oil and Gas Recovery of Ministry of Education, Northeast Petroleum University, Daqing 163318, China; piyanfu@163.com (Y.P.)
[2] Jiangsu Oilfield Engineering Institute, Yangzhou 225009, China
[3] China Petroleum and Chemical Corporation Shengli Oilfield Branch, Dezhou 256300, China
* Correspondence: suzailai2023@163.com

Abstract: This study investigated the impact of formation water on the mass transfer between CO_2 and crude oil in low-permeability reservoirs through CO_2 miscible flooding. Formation water leads to water blocks, which affect the effectiveness of CO_2 miscible flooding. Therefore, we studied the impact and mechanisms of formation water on the CO_2-oil miscibility. The microscale interaction between formation water-CO_2-core samples was investigated using CT scanning technology to analyze its influence on core permeability parameters. In addition, CO_2 miscible flooding experiments were conducted using the core displacement method to determine the effects of formation water salinity and average water saturation on minimum miscibility pressure (MMP) and oil displacement efficiency. The CT scanning results indicate that high-salinity formation water leads to a decrease in the porosity and permeability of the core as well as pore and throat sizes under miscible pressure conditions. The experimental results of CO_2 miscible flooding demonstrate that CO_2-oil MMP decreases as the salinity of the formation water increases. Moreover, as the average water saturation in the core increases, the water block effect strengthens, resulting in an increase in MMP. The recovery factors of cores with average water saturations of 30%, 45%, and 60% are 89.8%, 88.6%, and 87.5%, respectively, indicating that the water block effect lowers the oil displacement efficiency and miscibility.

Keywords: CO_2 miscible flooding; formation water salinity; water saturation; rock pore structure; minimum miscibility pressure

Citation: Pi, Y.; Su, Z.; Liu, L.; Wang, Y.; Zhang, S.; Li, Z.; Zhou, Y. Investigation of the Influence of Formation Water on the Efficiency of CO_2 Miscible Flooding at the Core Scale. *Processes* **2023**, *11*, 2954. https://doi.org/10.3390/pr11102954

Academic Editors: Qingbang Meng, Bin Liang, Zhan Meng and Yidong Cai

Received: 12 September 2023
Revised: 4 October 2023
Accepted: 9 October 2023
Published: 12 October 2023

1. Introduction

Low-permeability and ultra-low-permeability reservoirs account for a large proportion of China's proven reserves, which are highly valuable for exploitation due to their large reserves. Oil production from unconventional (low and ultra-low permeability) reservoirs ensures stable oil production in China [1,2]. CO_2 flooding is a proven enhanced oil recovery (EOR) technique in conventional reservoirs. The mechanisms of CO_2 flooding include viscosity reduction, swelling, miscibility, and re-energized reservoirs. Due to the nature of CO_2, it can be effectively utilized in tight oil and low-permeability reservoirs to improve oil recovery [3]. In addition, CO_2 injection is an important part of CO_2 utilization and storage to achieve the "dual carbon" goal [1,3]. CO_2 flooding can be classified as miscible flooding and immiscible flooding based on the minimum miscibility pressure (MMP) [4,5]. When the injection pressure is above the MMP, the CO_2 flooding is miscible flooding. CO_2 and crude oil undergo multiple contacts in miscible flooding, exchanging mass via evaporation and condensation and finally becoming miscible in one phase. Typically, CO_2 miscible flooding is applied in oilfields after water flooding in China's domestic reservoirs. Additionally, 67% of CO_2 flooding applications were conducted after water flooding, according to statistics on CO_2 flooding projects in the United States [6]. Therefore, CO_2 flooding technology is an effective method to further enhance the oil recovery of water-flooded reservoirs. Water blocks are formed in reservoirs by either formation water or injected water through water flooding, blocking the mass transfer between CO_2 and reservoir oil [7,8]. Although water does not directly participate in the miscibility process and mass transfer of oil and gas, it indirectly affects the extraction and diffusion between the oil and gas phases.

Currently, research on CO_2 flooding focuses on migration characteristics, influencing factors of CO_2 flooding, and minimum miscibility pressure, but there is a lack of research targeting the impact of formation water. After CO_2 is injected into a reservoir, it reacts with the formation water to form carbonic acid, which causes changes in pore structure. He et al. [9] studied water–rock interaction in the CO_2 flooding process. They found that this interaction could reduce the permeability of natural fractures near the injection well, leading to improved CO_2 flooding efficiency in the fractured reservoirs. Shiraki et al. [10] investigated the main reactions occurring in rock during the CO_2 flooding process. Soong et al. [11] analyzed the rock composition during CO_2 storage in saline aquifers and found a decrease in permeability. Wdowin et al. [12] observed mineral precipitation and dissolution in rock samples before and after CO_2 sequestration using scanning electron microscopy. These studies confirmed that formation water has a negative impact on reservoir structure.

Additionally, water affects various parameters in the CO_2 flooding process based on the literature. Li et al. [13] claimed that CO_2 could reduce the interfacial tension between oil and water, resulting in enhanced oil recovery. However, the alternating gas–water effects hindered the formation of the miscible zone and CO_2-oil miscibility. They also found that injecting appropriate gas plugs could reduce the impact of water on miscibility and significantly improve oil recovery through capillary experiments and numerical simulations [14]. Lv et al. [15] used a microscopic visualization model to study the effect of high water saturation on CO_2 flooding. They concluded that high water saturation blocked the contact between CO_2 and oil, delaying miscibility and prolonging the CO_2 EOR starting time. Tang et al. [16] studied the influence of CO_2 dissolution in formation water during oil displacement using thermodynamic models. The solubility of CO_2 in water was one order of magnitude larger than that of conventional hydrocarbons, resulting in a delay in gas breakthrough time and a 6% difference in oil recovery. Hu et al. [17] investigated the mass transfer mechanisms of water flooding and CO_2 flooding, indicating that CO_2 and crude oil could become miscible under different water saturations. However, high water saturation hindered mass transfer between the oil and gas phases. Liang et al. [18] studied the influence of bound water on gravity drainage under different mixed-phase conditions, finding that bound water reduced the recovery factor under immiscible conditions but increased the recovery of gravity drainage. For the study of the water block effect formed between CO_2 and crude oil, Qin [19] used a micro-visual model to investigate the oil displacement mechanism of CO_2-penetrating water. They found that CO_2 could penetrate the water block, change the wettability between oil and pores, and displace residual oil through column and cylindrical flows in high water saturation regions. Cui et al. [20] indicated that a thicker water film prolonged the time for oil and CO_2 to become miscible through microscopic visualization experiments. Torabi et al. [21] simulated water-alternating-gas injections and found that the solubility of CO_2 in water decreased with reduced CO_2 concentrations, leading to a delay in the oil recovery increment. Kazemi et al. [22] studied the effects of viscosity, gravity, and capillary forces under different miscible and bound water conditions, concluding that the presence of water led to pore throat blocking in near-miscible flooding. Pi et al. [23] studied the interaction between CO_2, rock, and formation water, and the experimental results showed that an increase in formation water salinity reduced the CO_2-oil MMP.

The literature confirms that CO_2 and crude oil become miscible via diffusion. Du et al. [24] studied the effect of nanoconfinement on the CO_2 diffusion coefficient in shale oil reservoirs. They calculated the effective diffusion coefficient in porous media by combining the properties of the reservoir. Hoteit et al. [25,26] used numerical simulation to investigate gas injection and recovery factors in fractured and non-fractured reservoirs. They concluded that diffusion had a minimal impact on gas injection efficiency. Li et al. [27] studied oil swelling in porous media due to CO_2 diffusion and matched experimental pressure curves with mathematical models to determine the effective diffusion coefficient. Mehdi et al. [28] proposed that the solubility of CO_2 in movable oil and connate oil would affect EOR based on numerical studies using artificial intelligence technology.

Currently, the influence of formation water on reservoirs mainly focuses on the carbon sequestration area, and there is a lack of in-depth study on the variation of pore–throat parameters when CO_2 becomes miscible. Generally, water blocks have an impact on CO_2 flooding, but the degree of their influence has not been quantified. The water block effect on CO_2 flooding in the miscible state must urgently be studied. In this study, CT scanning technology was used to study the influence of CO_2-water-rock interactions on the physical properties of the core under the pressure of a miscible state. Miscible flooding experiments of CO_2 were conducted on core samples under different average water saturation conditions to reveal the effects of water blocks on CO_2 flooding. In addition, the minimum miscible pressure between CO_2 and crude oil was obtained via experimental measurements. The findings provide insights into the implementation of CO_2 flooding in the field.

2. Experimental Materials and Methods

2.1. Experimental Materials

Experimental instruments: 1172 micro-CT micro-focus computer scanner (produced by Belgian Sky Scan company, Skyscan, Belgium) with a resolution of 1.0 μm and a maximum X-ray voltage of 100 kV; Teledyne ISCO 260D high-pressure, high-precision syringe pump (produced by American Edyne Isco company, Lincoln, NH, USA) with a flow rate of 0.001–107 mL/min and a pressure of 10–7500 psi; STY-2 gas permeability tester (produced by Haian Petroleum Research Instrument Co., Ltd., Haian, China), with a permeability test range of 0.01×10^{-3} μm^2 to 6 μm^2.

Experimental oil: Simulated oil with a viscosity of 1.21 mPa·s, volume coefficient of 1.313, gas–oil ratio of 78.35 m^3/m^3, density of 0.7365 g/cm^3, saturation pressure of 11.72 MPa, and experimentally measured minimum miscible pressure of 20.17 MPa.

Experimental water: Distilled water and simulated formation water, with the chemical agent ratio for simulated formation water shown in Table 1.

Table 1. Composition of simulated formation water.

Compositions	Na_2SO_4	NaCl	Na_2CO_3	$NaHCO_3$	$CaCl_2$	$MgCl_2 \cdot 6H_2O$	Salinity (g/L)
Concentration (g/L)	0.0139	0.3835	0.0539	2.262	0.01385	0.04182	2.769
	0.028	0.77	0.108	4.52	0.028	0.084	5.538

Experimental gas: Industrial-grade CO_2 gas (purity 99%). Experimental temperature: 69.05 °C.

Experimental core: 12 Berea cylindrical cores (core parameters shown in Table 2).

Table 2. Physical properties of cores.

Core Number	Length (cm)	Cross-Sectional Area (cm^2)	Permeability ($\times 10^{-3}$ μm^2)	Porosity (%)
A1	30.15	4.91	5.1	12.5
A2	30.12	4.91	5.3	12.8
A3	30.13	4.91	4.9	12.3
B1	30.54	4.91	5.3	12.7
B2	30.57	4.91	5.2	15.4

2.2. Experimental Methods

2.2.1. CO_2 Soaking Experiment

In order to study the interactions between CO_2-water-rock during CO_2 miscible flooding, CO_2 soaking experiments were performed using Berea cores. The interactions caused changes in pore-permeability parameters and ultimately affected CO_2-oil miscibility. After saturating the cores with formation water with varying degrees of mineralization, the CO_2 was injected under miscible pressure to study the variation patterns of pore-permeability parameters of the rocks. The 30 cm Berea cores were cut following the cutting plan shown in Figure 1. The soaking plans for CO_2 are presented in Table 3.

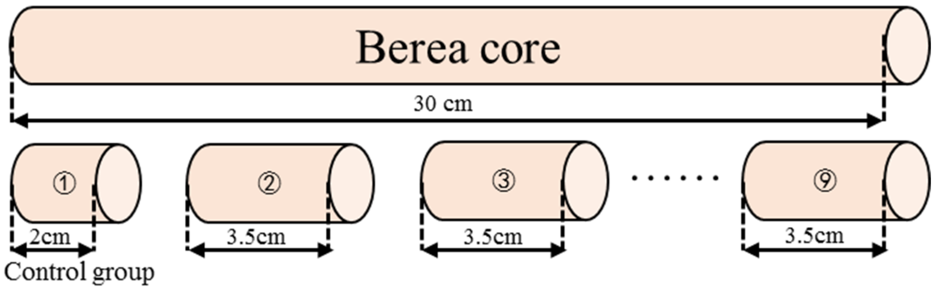

Figure 1. Schematic diagram of Berea core cutting.

Table 3. Soaking well plan for CO_2.

Core Number	Program					
	Experimental Preparation	**Plan 1**	**Plan 2**	**Plan 3**	...	**Plan 8**
A1	Saturated with distilled water, then injected with CO_2 and soaked for varying times.	Soaking 6 h	Soaking 12 h	Soaking 18 h	...	Soaking 48 h
A2	Saturated with 2.769 g/L formation water, then injected with CO_2 and soaked for varying times.					
A3	Saturated with 5.538 g/L formation, then injected with CO_2 and soaked for varying times.					

The experimental procedure of the CO_2 soaking experiment is as follows:

(1) Weigh the Berea core, measure the original air permeability, saturate it with distilled water after vacuuming, and measure the original core porosity.
(2) Dry the core in a constant-temperature oven for 48 h, cut the cores according to the plan (Figure 1), and label the cores as No. 1 to No. 9.
(3) Scan the cross-section of core No. 1 (acting as the control group) using CT to record the distribution of the pore–throat radius in the core. Saturate cores No. 2 to No. 9 with simulated formation water after vacuuming, and soak the cores corresponding to experimental plans 1 to 8. The experimental setup (as shown in Figure 2) is used to inject CO_2, reach the experimental pressure of 21 MPa, and achieve various soaking times indicated in the experimental plans.
(4) After soaking, slowly depressurize, remove the cores, and dry them in an oven for 48 h. Measure the air permeability and then saturate with distilled water to measure the porosity.
(5) Take the Berea core from experimental plan 8, cut it into slices, and scan the cross-section using CT to record the distribution of the core pore–throat radius.

2.2.2. CO_2 Flooding Experiments under Different Water Saturation Conditions

Water always exists in reservoirs and affects the miscibility of CO_2 and crude oil via the water block effect. In this experiment, we evaluated the impact of the water block effect on miscible CO_2 and crude oil using different average water saturation cores. The average water saturation represents the strength of the water block effect. The CO_2 flooding experimental schemes are presented in Table 4, and the experimental setup is the same as that shown in Figure 2.

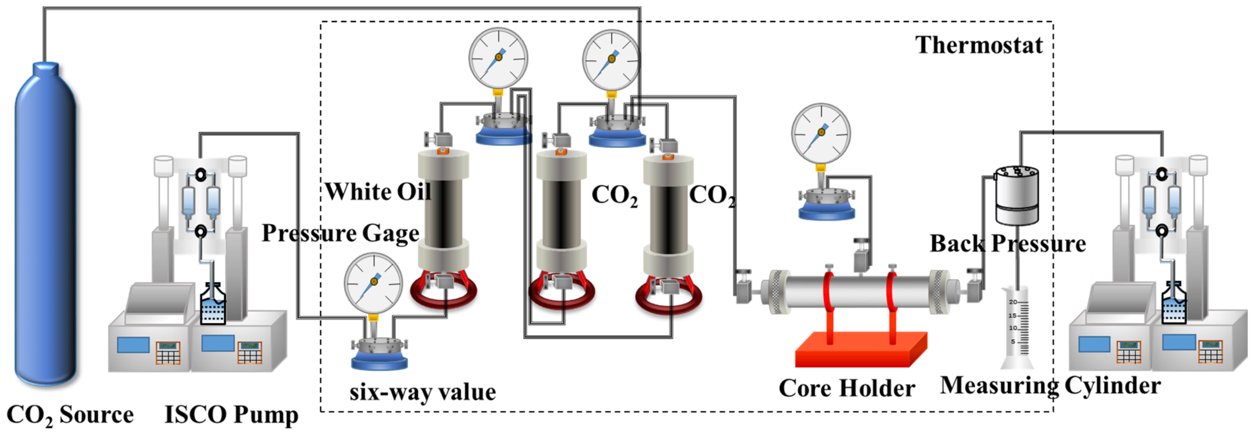

Figure 2. Experimental setup.

Table 4. CO_2 flooding experimental schemes under different water saturation conditions.

Scheme Number	Plan Details	
1	Saturate with distilled water to achieve 30% average water saturation	CO_2 flooding experimental pressure: 5 MPa, 10 MPa, 15 MPa, 20 MPa, 25 MPa, 30 MPa, and 35 MPa
2	Saturate with formation water with a salinity of 2.769 g/L to achieve 30% average water saturation	
3	Saturate with formation water with a salinity of 5.538 g/L to achieve 30% average water saturation	
4	Saturate with distilled water to achieve 45% average water saturation	
5	Saturate with formation water with a salinity of 2.769 g/L to achieve 45% average water saturation	
6	Saturate with formation water with a salinity of 5.538 g/L to achieve 45% average water saturation	
7	Saturate with distilled water to achieve 60% average water saturation	
8	Saturate with formation water with a salinity of 2.769 g/L to achieve 60% average water saturation	
9	Saturate with formation water with a salinity of 5.538 g/L to achieve 60% average water saturation	

The experimental procedure of the CO_2 flooding experiment is presented below:

(1) Weigh the Berea rock core under dry conditions, vacuum the core, and saturate it with simulated oil to calculate the porosity of the rock core.
(2) Connect the experimental setup, conduct water flooding with an injection rate of 0.3 mL/min, and terminate water injection after reaching the target water saturation according to the experimental plan.
(3) Conduct CO_2 flooding experiments with a 0.3 mL/min rate and adjust the back pressure valve pressure according to the experimental plan. Record the oil production and calculate the recovery factor when no oil is produced under this pressure condition.
(4) Adjust the pressure of the back pressure valve to the next pressure point, increase the injection pressure above the experimental pressure, and continue the CO_2 flooding experiment. Complete the CO_2 flooding experiment after finishing testing all 7 experimental pressures.

3. Results and Discussion

3.1. Changes in Porosity and Permeability

The changes in the porosity and permeability of the Berea rock core after being saturated with different simulated formation water levels and various CO_2 soaking times are shown in Figures 3 and 4. The porosity and permeability of the Berea rock core initially increase and then decrease with soak time. For the core saturated with distilled water, the ultimate porosity and permeability slightly increase compared to its original state. However, the cores saturated with simulated formation water decrease in both porosity and permeability. The higher the salinity, the more significant the decrease in porosity and permeability. The cores saturated with water of salinity 2.769 g/L and 5.538 g/L lead to a decrease in porosity by 2% and 2.7% and a decrease in permeability by 1.5×10^{-3} μm^2 and 2.4×10^{-3} μm^2, respectively.

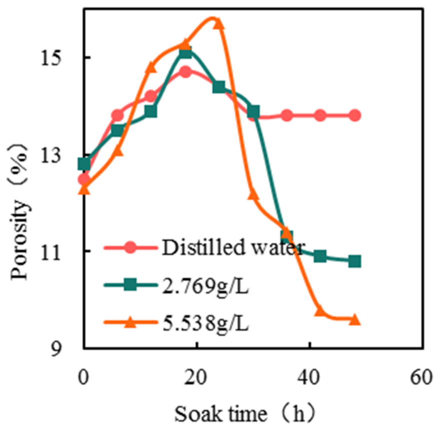

Figure 3. Variation of porosity with soak time.

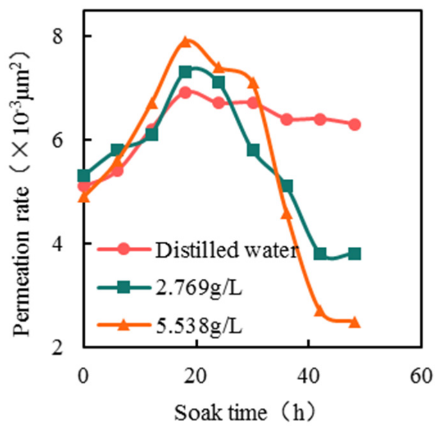

Figure 4. Variation of permeability with soak time.

The main mineral components of the cores are quartz, potassium feldspar, plagioclase, clay minerals, and carbonate minerals (calcite, dolomite, and aragonite). CO_2 dissolves in water to form carbonic acid through the reaction shown in the chemical Equation (1). The corrosiveness of carbonic acid increases as pressure in multiphase conditions increases, leading to dissolution reactions with calcite and dolomite [29,30]. Chemical Equations (2) and (3) show the chemical changes resulting from these reactions. As the reactions continue, the dissolution of the above components leads to an increase in the concentration of calcium and magnesium ions. Followed by precipitation reactions, calcium and magnesium ions gradually react with bicarbonate ions in the formation water to form insoluble carbonates, as shown in chemical Equations (4) and (5).

$$CO_2 + H_2O = HCO_3^- + H^+ \tag{1}$$

$$CaMg(CO_3)_2 + 2H^+ = Ca^{2+} + Mg^{2+} + 2HCO_3^- \tag{2}$$

$$Ca(Fe_{0.7}Mg_{0.3})(CO_3)_2 + 2H^+ = Ca^{2+} + 0.3Mg^{2+} + 0.7Fe^{2+} + 2HCO_3^- \tag{3}$$

$$Mg^{2+} + HCO_3^- = MgCO_3 \downarrow + H^+ \tag{4}$$

$$Ca^{2+} + HCO_3^- = CaCO_3 \downarrow + H^+ \tag{5}$$

The analysis results suggest that the higher the mineralization, the lower the solubility of CO_2 in water. For the core saturated with distilled water, the acidity of carbonic acid is enhanced, increasing the dissolution effect on the reservoir and generating numerous secondary pores. However, the subsequent precipitation of insoluble carbonates gradually migrates to smaller pore throats, blocking the channels with smaller radii. Pi et al. [23] studied the reaction among CO_2, formation water, and rock. The dissolution of CO_2 in the formation water resulted in a decrease in the pH of the formation water from 7.4 to 6.5. With the continued injection of CO_2, the pH of the formation water increased and then decreased. In general, cores saturated with distilled water have lower mineral ion concentrations, dominated by dissolution, resulting in a slight increase in overall porosity and permeability. In contrast, cores saturated with formation water have higher calcium and magnesium ion concentrations, with precipitation dominating, leading to a significant decrease in overall porosity and permeability. Due to the utilization of low-permeability cores in the experiment, alterations in both porosity and permeability exhibit a significantly more noticeable impact.

The CT scan results of the core after 48 h of soaking are shown in Figure 5. The porosity of the core saturated with distilled water is slightly larger than that of the control group. After saturation with formation water with different salinity levels, both the pores and pore throats decrease in size—higher salinity results in larger changes. As a result of precipitation, the dimensions of the primary large pores undergo a noticeable reduction, while numerous secondary pores emerge, thereby instigating substantial alterations in porosity.

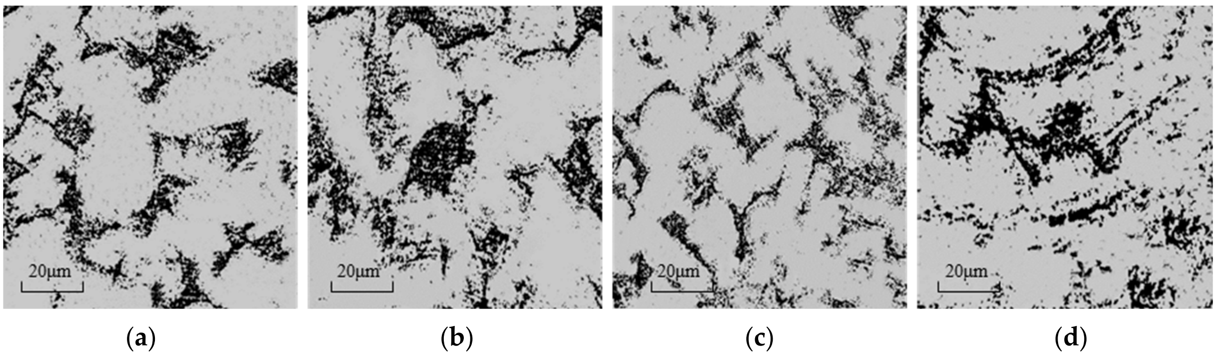

Figure 5. Core CT scan after CO_2 soaking for 48 h. (**a**) Original core, (**b**) saturated with distilled water, (**c**) saturated with formation water (salinity of 2.769 g/L), and (**d**) saturated with formation water (salinity of 5.538 g/L).

3.2. Distribution of Pore Radius and Throat Radius

The distribution of the core's pore radius and throat radius after 48 h of CO_2 soaking was calculated, and the experimental results are shown in Figures 6–9.

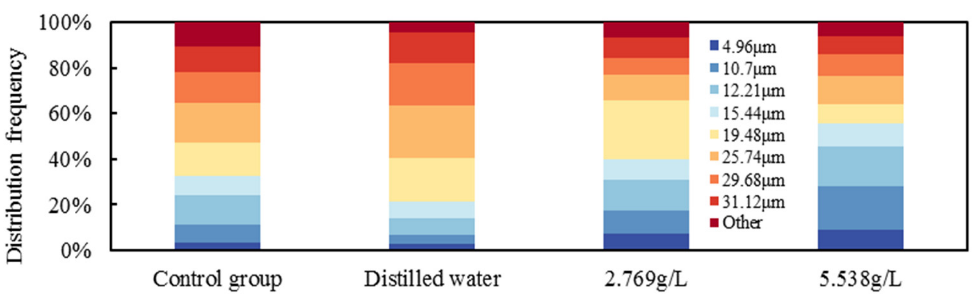

Figure 6. Distribution of pore radius.

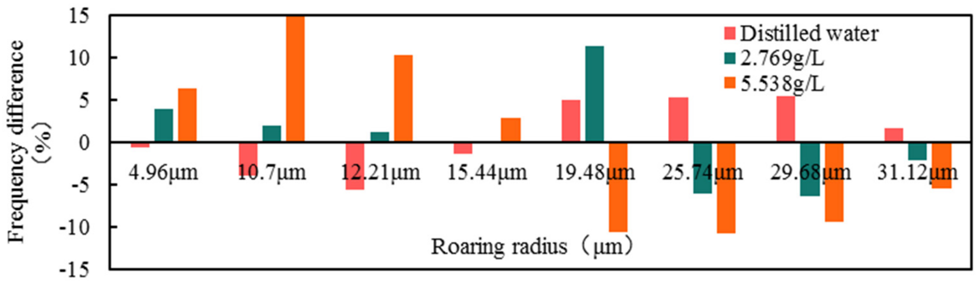

Figure 7. Frequency difference of pore radius.

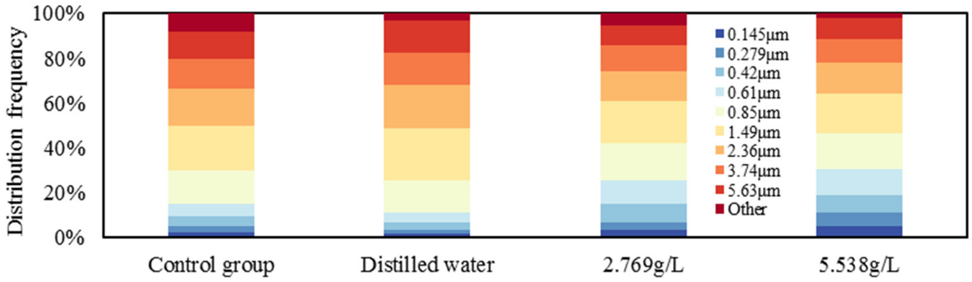

Figure 8. Distribution of pore throat radius.

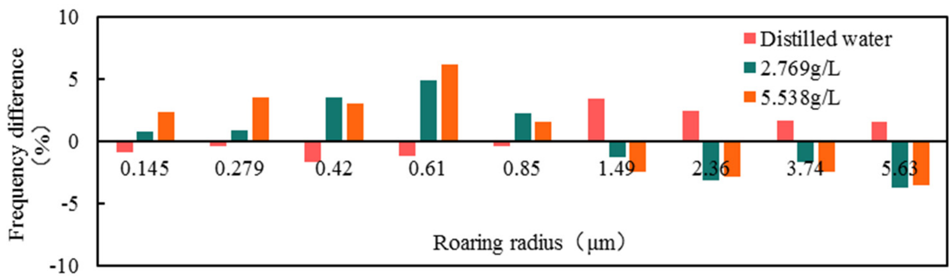

Figure 9. Frequency difference of pore throat radius.

After 48 h of soaking in saturated distilled water, the distribution of pore radii below 15.44 μm decreases, while the distribution of pore radii above 19.48 μm increases for the Berea cores. In addition, for cores saturated with formation water with a salinity of 2.769 g/L and 5.538 g/L, the distribution of pore radii below 19.48 μm increases, while the distribution of pore radii above 19.48 μm decreases. Therefore, higher salinity results in a higher distribution of small-size pores. The pattern of throat radius distribution is consistent with that of pore radius distribution, and the distribution of small throats increases as salinity increases. These observations indicate that increasing salinity gradually alters the dominant factor in the pore and throat radius from dissolution to precipitation, causing the blockage of large pores and an increase in the distribution of small pores.

3.3. MMP Alterations under Different Water Saturations

Figure 10 shows the results of MMP experiments at different average water saturations. The MMPs were determined using the slim tube experiment, which was obtained by intersecting the trend lines of the immiscible region recovery rate and the miscible region recovery rate. This experimental pressure represents the minimum pressure required to achieve maximum recovery under different water block conditions. The results indicate that the MMP between CO_2 and oil decreases as the salinity of the formation water increases, and a stronger water block effect (higher average water saturation) leads to a higher MMP. When the average water saturation of the cores is 30%, the obtained MMP values of distilled water, salinity of 2.769 g/L, and salinity of 5.538 g/L scenarios are 20.73 MPa, 20.27 MPa, and 19.33 MPa, respectively. As the average water saturation increases to 45%, the MMP values are 21.25 MPa, 20.66 MPa, and 19.65 MPa, respectively. Further increasing the average water saturation to 60%, the MMP values are 21.89 MPa, 21.01 MPa, and 19.97 MPa, respectively.

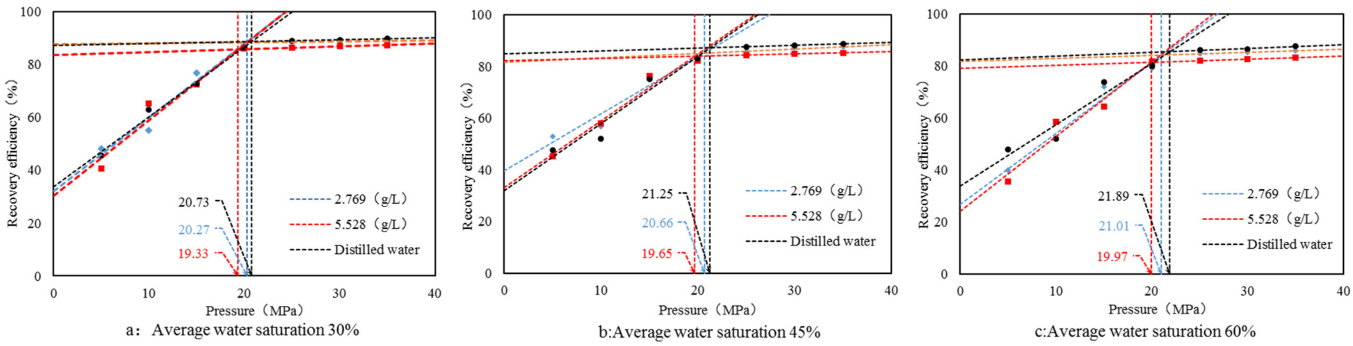

Figure 10. Minimum miscibility pressure under different average water saturations.

Based on the above results, it can be concluded that the salinity of formation water affects the pore–throat structure of the core under miscible pressure, resulting in a decrease in porosity and an increase in small pore channels. The contact surface between oil, gas, and water phases is segmented and compressed, leading to intense mass transfer between CO_2 and crude oil and a slight decrease in MMP.

3.4. Changes in Oil Displacement Effect under Different Water Saturation

The oil recovery of CO_2 miscible flooding experiments is shown in Table 5. The stronger the water block effect, the lower the oil recovery. The average water saturation increases from 30% to 60%. The core samples saturated with distilled water and formation water with a salinity of 2.769 g/L and 5.538 g/L show a decrement in oil recovery of 2.3%, 3.3%, and 4.1%, respectively. These recovery factor decreases are caused by three reasons: (1) The water phase is the wetting phase, which easily enters the small pore throat and traps the residual oil at the dead-end. This phenomenon increases the difficulty of oil recovery, leading to a lower recovery factor. (2) Water affects the mass transfer process between CO_2 and crude oil as the water block effect strengthens, changing the contact mode from direct contact to indirect contact that CO_2 dissolves in water and then comes into contact with crude oil. This change reduces the contact area and decreases the efficiency of miscible flooding. (3) The water block increases MMP and reduces the miscibility, resulting in lower oil recovery. The impact of the formation water salinity on oil recovery is analyzed as follows: the increase in secondary pores enhances the complexity of dead-end residual oil, making it challenging to recover crude oil from dead-end pores and eventually reducing the overall oil recovery.

Table 5. Recovery factors of CO_2 miscible flooding experiments.

Category	Recovery Factors (%)		
	Distilled Water	Salinity of 2.769 g/L	Salinity of 5.538 g/L
Average water saturation 30%	89.8	89.1	87.4
Average water saturation 45%	88.6	87.4	85.2
Average water saturation 45%	87.5	85.8	83.3

4. Conclusions

(1) In the case of miscible flooding, highly mineralized formation water can enhance precipitation, resulting in a decrease in core porosity and permeability as well as a reduction in pore and throat size.
(2) The higher the average water saturation of the core, the stronger the water block effect and the higher the MMP. However, the formation water with high salinity can decrease the MMP between CO_2 and crude oil. Overall, the impact of the formation water's salinity is greater than the impact of the average water saturation of the core.
(3) The average water saturation impacts the oil displacement and the miscible behavior of CO_2 for three reasons: an increase in the proportion of residual oil in dead-end pores, a decrease in the oil displacement efficiency of CO_2 with crude oil, and a decrease in the miscibility. Additionally, the decrease in porosity and permeability of the reservoir makes it challenging to extract the crude oil, thereby affecting the oil displacement.

Author Contributions: Conceptualization, Y.P. and Z.S.; methodology, Y.P. and Z.S.; formal analysis, L.L. and Y.W.; data curation, Z.L. and Y.Z.; writing—original draft preparation, Z.S. and S.Z.; writing—review and editing, L.L.; funding acquisition, Y.P. All authors have read and agreed to the published version of the manuscript.

Funding: This work was supported by the National Natural Science Foundation of China (No. 52174023) and the Natural Science Foundation of Heilongjiang Province (No. LH2021E015).

Data Availability Statement: The authors confirm that the data supporting the findings of this study are available within the article.

Acknowledgments: The authors are grateful for the support from all laboratory technicians.

Conflicts of Interest: The authors declare no conflict of interest.

References

1. Song, X.; Wang, F.; Ma, D.; Gao, M.; Zhang, Y. Progress and prospect of carbon dioxide capture, utilization and storage in CNPC oilfields. *Pet. Explor. Dev.* **2023**, *50*, 206–218. [CrossRef]
2. Yang, Y.B.; Xiao, W.L.; Bernabe, Y.; Xie, Q.; Wang, J.; He, Y.; Li, M.; Chen, M.; Ren, J.; Zhao, J.; et al. Effect of pore structure and injection pressure on waterflooding in tight oil sandstone cores using NMR technique and pore network simulation. *J. Pet. Sci. Eng.* **2022**, *217*, 110886. [CrossRef]
3. Liao, G.; He, D.; Wang, G.; Wang, L.; Wang, Z.; Su, C.; Qin, Q.; Bai, J.; Hu, Z.; Huang, Z.; et al. Discussion on the limit recovery factor of carbon dioxide flooding in a permanent sequestration scenario. *Pet. Explor. Dev.* **2022**, *49*, 1262–1268. [CrossRef]
4. Ghomian, Y.; Pope, G.A.; Sepehrnoori, K. Reservoir simulation of COMK sequestration pilot in Frio brine formation, USA Gulf Coast. *Energy* **2008**, *33*, 1055–1067. [CrossRef]
5. Zhang, N.; Yin, M.F.; Wei, M.Z.; Bai, B.J. Identification of COMK sequestration opportunities: COMK miscible flooding guidelines. *Fuel* **2019**, *241*, 459–467. [CrossRef]
6. Qin, J.; Han, H.; Liu, X. Application and enlightenment of carbon dioxide flooding in the United States of America. *Pet. Explor. Dev.* **2015**, *42*, 209–216. [CrossRef]
7. Chen, H.; Liu, X.; Jia, N.; Zhang, K.; Yang, R. Key scientific issues and prospects of CO_2 near miscible flooding. *Pet. Sci. Bull.* **2016**, *3*, 1–10.
8. Trivedi, J.; Babadagli, T. Efficiency analysis of greenhouse gas sequestration during miscible CO_2 injection in fractured oil reservoirs. *Environ. Sci. Technol.* **2008**, *42*, 5473–5479. [CrossRef]
9. He, Y.F.; Ji, B.Y.; Yang, S.; Liu, X.; Zhao, S.X.; Zhou, Y.L. Water-rock-CO_2 interactions and CO_2 storage of Honghe tight oil reservoirs: An experimental and simulation study. *Greenh. Gases-Sci. Technol.* **2019**, *9*, 703–718. [CrossRef]
10. Shiraki, R.; Dunn, T.L. Experimental study on water-rock interactions during CO_2 flooding in the Tensleep Formation, Wyoming, USA. *Appl. Geochem.* **2000**, *15*, 265–279. [CrossRef]
11. Soong, Y.; Howard, B.H.; Dilmore, R.M.; Haljasmaa, I.; Crandall, D.M.; Zhang, L.W.; Zhang, W.; Lin, R.H.; Irdi, G.A.; Romanov, V.N.; et al. CO_2/brine/rock interactions in Lower Tuscaloosa formation. *Greenh. Gases Sci. Technol.* **2016**, *6*, 824–837. [CrossRef]
12. Wdowin, M.; Franus, W. *Determination of CO_2-Brine-Rock Interactions for Carbon Dioxide Sequestration Using SEM-EDS Methods*; Springer: Berlin/Heidelberg, Germany, 2016; pp. 119–133.
13. Li, M.; Shan, W.; Liu, X. Experimental Study on the Mechanism of Supercritical Carbon Dioxide Mixed Phase Oil Displacement. *Acta Pet. Sin.* **2006**, *27*, 80–83.

14. Li, M.; Zhang, Y.; Yang, Z.; Liu, X.; Yao, S. Research on CO_2 miscible flooding to enhance oil recovery in low permeability reservoir. *Oil Drill. Prod. Technol.* **2005**, *27*, 43–46.
15. Lu, C.; Wang, R.; Cui, M.; Tang, Y.; Zhou, X. Displacement experiment of CO_2 miscible flooding under high water condition. *Acta Pet. Sin.* **2017**, *38*, 1293–1298.
16. Tang, Y.; Du, Z.; Sun, L.; Liu, W.; Chen, Z. Influence of CO_2 dissolving in formation water on CO_2 flooding process. *Acta Pet. Sin.* **2011**, *32*, 311–314.
17. Hu, W.; Lu, C.; Wang, R.; Cui, M.; Yang, Y.; Wang, X. Porous flow mechanisms and mass transfer characteristics of CO_2 miscible flooding after water flooding. *Acta Pet. Sin.* **2018**, *39*, 201–207.
18. Liang, J.; Quan, G. The Effect of Condensate Film on Oil Release Rate in Horizontal Well Steam Assisted Gravity Oil Release. *J. Pet. Univ. (Nat. Sci. Ed.)* **2001**, *6*, 52–54+57. [CrossRef]
19. Qin, J.; Zhang, K.; Chen, X. Mechanism of the CO_2 flooding as reservoirs containing high water. *Acta Pet. Sin.* **2010**, *31*, 797–800.
20. Cui, M.; Wang, R.; Lv, C.; Tang, Y. Research on microscopic oil displacement mechanism of CO_2 EOR in extra-high water cut reservoirs. *J. Pet. Sci. Eng.* **2017**, *154*, 315–321. [CrossRef]
21. Torabi, F.; Jamaloei, B.Y.; Zarivnyy, O.; Paquin, B.A.; Rumpel, N.J. The Evaluation of Variable-Injection Rate Waterflooding, Immiscible CO_2 Flooding, and Water-alternating-CO_2 Injection for Heavy Oil Recovery. *Pet. Sci. Technol.* **2012**, *30*, 1656–1669. [CrossRef]
22. Kazemi, K.; Rostami, B.; Khosravi, M.; Bejestani, D.Z. Effect of Initial Water Saturation on Bypassed Oil Recovery during CO_2 Injection at Different Miscibility Conditions. *Energy Fuels* **2015**, *29*, 4114–4121. [CrossRef]
23. Pi, Y.F.; Liu, J.X.; Liu, L.; Guo, X.; Li, C.L.; Li, Z.H. The Effect of Formation Water Salinity on the Minimum Miscibility Pressure of CO_2-Crude Oil for Y Oilfield. *Front. Earth Sci.* **2021**, *9*, 711695. [CrossRef]
24. Du, F.S.; Nojabaei, B. Estimating diffusion coefficients of shale oil, gas, and condensate with nano-confinement effect. *J. Pet. Sci. Eng.* **2020**, *193*, 107362. [CrossRef]
25. Hoteit, H.; Firoozabadi, A. Numerical Modeling of Diffusion in Fractured Media for Gas-Injection and -Recycling Schemes. *SPE J.* **2009**, *14*, 323–337. [CrossRef]
26. Hoteit, H. Modeling diffusion and gas-oil mass transfer in fractured reservoirs. *J. Pet. Sci. Eng.* **2013**, *105*, 1–17. [CrossRef]
27. Li, Z.W.; Dong, M.Z. Experimental Study of Carbon Dioxide Diffusion in Oil-Saturated Porous Media under Reservoir Conditions. *Ind. Eng. Chem. Res.* **2009**, *48*, 9307–9317. [CrossRef]
28. Mahdaviara, M.; Amar, M.N.; Hemmati-Sarapardeh, A.; Dai, Z.X.; Zhang, C.S.; Xiao, T.; Zhang, X.Y. Toward smart schemes for modeling CO_2 solubility in crude oil: Application to carbon dioxide enhanced oil recovery. *Fuel* **2021**, *285*, 119147. [CrossRef]
29. Miller, J.P. A portion of the system calcium carbonate-carbon dioxide-water, with geological implications. *Am. J. Sci.* **1952**, *250*, 161–203. [CrossRef]
30. Busenberg, E.; Plummer, L.N. The kinetics of dissolution of dolomite in CO_2-H_2O systems at 1.5 to 65 degrees C and O to 1 atm PCO_2. *Am. J. Sci.* **1982**, *282*, 45–78. [CrossRef]